Frontiers of Information Technology & Electronic Engineering
www.jzus.zju.edu.cn; engineering.cae.cn; www.springerlink.com
ISSN 2095-9184 (print); ISSN 2095-9230 (online)
E-mail: jzus@zju.edu.cn

Design, development, and performance of an ammonia self-managed vaporization propulsion system for micro-nano satellites*

Shu-jian SUN†, Tao MENG†‡, Zhong-he JIN

School of Aeronautics and Astronautics, Zhejiang University, Hangzhou 310027, China

†E-mail: sunshujian@zju.edu.cn; mengtao@zju.edu.cn

Received Jan. 25, 2018; Revision accepted June 17, 2018; Crosschecked July 12, 2019; Published online Aug. 7, 2019

Abstract: An ammonia self-managed vaporization propulsion (ASVP) system for micro-nano satellites is presented. Compared with a normal cold gas or liquefied gas propulsion system, a multiplex parallel sieve type vaporizer and related vaporization control methods are put forward to achieve self-managed vaporization of liquefied propellant. The problems of high vaporization latent heat and incomplete vaporization of liquefied ammonia are solved, so that the ASVP system takes great advantage of high theoretical specific impulse and high propellant storage density. Furthermore, the ASVP operation procedure and its physical chemistry theories and mathematical models are thoroughly analyzed. An optimal strategy of thrust control is proposed with consideration of thrust performance and energy efficiency. The ground tests indicate that the ASVP system weighs 1.8 kg (with 0.34-kg liquefied ammonia propellant) and reaches a specific impulse of more than 100 s, while the power consumption is less than 10 W. The ASVP system meets multiple requirements including high specific impulse, low power consumption, easy fabrication, and uniform adjustable thrust output, and thus is suitable for micro-nano satellites.

Key words: Self-managed vaporization; Liquefied ammonia; Milli-Newton level propulsion; Micro-thrust; High-precision orbital control; Micro-nano satellite

https://doi.org/10.1631/FITEE.1800068 **CLC number:** V439; TP23

1 Introduction

Micro-nano satellites have exhibited explosive growth in recent years due to their low cost, small volume, light weight, ease of massive production, and quick network construction. According to the "2017 State of the Satellite Industry Report" (Satellite Industry Association, 2017), more than 1000 micro-nano satellites were launched between 2000 and 2016. Beyond technical demonstration and space science experiments, the development of micro-nano satellites has entered a new stage of space applications (Poghosyan and Golkar, 2017). Particularly, micro-nano satellite constellation and formation flying have become the most promising development trends for further micro-nano satellite applications. All of these new applications need a milli-Newton (mN) level propulsion system for all aspects of their operations. A high-efficiency propulsion system will provide orbital-maneuvering, high-precision attitude control, and station-keeping capabilities at a low cost (Chigier and Gemci, 2003).

The most commonly used propulsion techniques for micro-nano satellites (Scharfe and Ketsdever, 2009; Lemmer, 2017) include cold gas propulsion, liquefied gas propulsion, electric propulsion, and chemical propulsion. An electric propulsion (Levchenko

‡ Corresponding author

* Project supported by the National Natural Science Foundation of China (No. 61503334) and the National Science Fund for Distinguished Young Scholars (No. 61525403)

ORCID: Shu-jian SUN, http://orcid.org/0000-0002-3016-4546

© Zhejiang University and Springer-Verlag GmbH Germany, part of Springer Nature 2019

et al., 2018) system offers incredibly high specific impulse, but the output thrust is very low (usually at a micro-Newton (μN) level) and the power consumption is high. Cold gas propulsion (Matticari et al., 2006; Ranjan et al., 2017) systems are simple structures and can be easily implemented, but their low propellant storage density causes limited total impulse. Chemical propulsion systems (Carpenter et al., 2013) use the chemical energy stored within a propellant to create propulsion; although many systems are under development, no micro-nano satellites with a chemical propulsion system have been launched (Lemmer, 2017). Compared with the above-mentioned propulsion systems, liquefied gas propulsion (Gibbon et al., 2000) systems are superior in thrust value, specific impulse, propellant storage density, and power consumption, and are a better choice for micro-nano satellites.

Among common liquefied gas propellants, liquefied ammonia (NH_3) has the highest theoretical specific impulse (Gibbon et al., 2001) and has been widely used. In Hejmanowski and Woodruff (2015), the characteristics of different propellants (including NH_3, N_2O, N_2H_4, SF_6, and C_4H_{10}) are compared. Ammonia has a high sound speed, is self-pressurizing, reaches a high critical temperature, and has a low freezing point. However, its high vaporization heat, not compatible with materials and electronics, and its low density, are the disadvantages that present difficulty in propulsion system design.

Researchers in related fields have suggested a series of propulsion systems to exploit the advantages and avoid the disadvantages of ammonia. Zube and Messerschmid (1993) introduced a 700-W ammonia arcjet propulsion system used on a P3D satellite, which was launched by the International Radio Amateur Organization AMSAT. The average output thrust value was 100 mN and the specific impulse reached 450 s. However, the total weight (7 kg without propellant tanks) and the high power consumption do not work for most micro-nano satellites. Guo et al. (2013) presented a design for the propulsion system for the YH-1 Mars probe. This system makes the liquefied ammonia vaporize by latent heat and uses a liquid-choke valve to prevent the liquid from flowing into the thrusters. The output specific impulse can be up to 103 s, but the output thrust value varies greatly based on the unstable inner pressure of the tank, which is governed by the vaporization rate. Wei and Li (2012) created a liquefied ammonia flashing jet propulsion system used in BX-1 (the circling satellite of Shenzhou-7 spacecraft). This propulsion system is simple in structure, high in thrust value (up to 860 mN), and low in power consumption (only the nozzle needs to be heated if it is going to freeze). Nevertheless, the principle of the flashing jet causes the liquefied ammonia to vaporize incompletely, so the output specific impulse is far below the theoretical specific impulse (only 34 s).

The propulsion systems mentioned above represent three frequently used methods for processing liquefied ammonia propellant.

1. Heated jet

The liquefied ammonia is heated to a very high temperature by a Hall thruster, an ion thruster, or a resistojet thruster (Robin et al., 2008; Lappas et al., 2011; Levchenko et al., 2018) to achieve high specific impulse. This kind of propulsion system usually has a large number of ancillary devices and a complex inner structure. In addition, the output thrust value is always very low despite the power consumption being high.

2. Gas-liquid separation

The liquefied ammonia vaporizes in a container and the gas separates from the liquid-gas mixture (Guo et al., 2013). This kind of propulsion system is often used as a blow-down system that will either lose energy unnecessarily or output unstable thrust. The system also takes more power to heat the propellant tank, and the vaporization energy cost is high.

3. Flashing jet

The liquefied ammonia flows directly through the thrusters and vaporizes at the nozzle to output thrust (Wei and Li, 2012). This kind of propulsion system has a very simple structure and requires less power. However, its output thrust fluctuates and the specific impulse is not ideal.

In summary, the existing liquefied ammonia propulsion techniques have solved the problems using liquefied ammonia propellant and the methods of producing thrust, which have been applied in many space missions. However, the defects in vaporization management make it impossible to fully and efficiently use the high specific impulse of ammonia in propulsion systems. To solve this problem, the design of the ammonia self-managed vaporization propulsion (ASVP) system is presented in this paper. A new multiplex parallel sieve type

vaporizer structure and related vaporization process control methods lead to the realization of a high specific impulse and uniform thrust pulse propulsion system, which is suitable for micro-nano satellites. Notations used in this paper are shown in Table 1.

2 Scheme of ammonia self-managed vaporization propulsion

The ASVP system is composed of an ammonia tank, a stop valve, a vaporizer, heaters, and thrusters. The schematic of the ASVP system is shown in Fig. 1. Liquefied ammonia propellant is stored in the ammonia tank, and the stop valve controls the flow of liquefied ammonia into the vaporizer. The propellant gets heat from the heaters that are attached to the vaporizer. Liquefied ammonia turns into gaseous ammonia and is ejected from the nozzle to produce thrust.

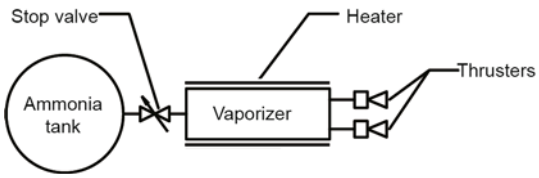

Fig. 1 General sketch of the ammonia self-managed vaporization propulsion (ASVP) prototype

The vaporizer is the lynchpin of the ASVP system and allows us to achieve propellant feedstock, vaporization management, and thrust control. The structure of the vaporizer is shown in Fig. 2.

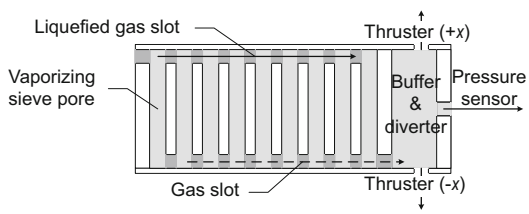

Fig. 2 Structure of the vaporizer

This structure is divided into four major parts: liquefied gas slot, gas slot, multiplex parallel vaporizing sieve pores, and buffer (diverter). The propellant flows into the liquefied gas slot and flows out the gas slot. The key vaporization process occurs when the propellant flows through the multiplex parallel vaporizing sieve pores. These sieve pores effectively enhance the contact area of the heat transfer between the vaporizer and the propellant, and the aluminum alloy structure increases heat capacity. Multiplex parallel pores maintain a uniform distribution of the inflow propellant so that the liquefied ammonia can be heated evenly. The vaporization process is efficient because the volume of inflow liquefied ammonia takes only part of the vaporizer capacity. The liquid always gathers in the liquefied gas slot and the gas always gathers in the gas slot, which ensures that the ammonia enters the thrusters in the gaseous state only. Accordingly, liquefied ammonia vaporizes

Table 1 Notations used in this paper

Notation	Definition
F	Value of thrust
I	Value of impulse
C_{f}	Thrust coefficient
P_{c}	Thrust chamber pressure
A_{t}	Nozzle throat area
I_{sp}	Specific impulse
I_{spt}	Theoretical specific impulse
$\dot{m}$	Propellant mass flow rate
T_{c}	Thrust chamber temperature
k	Specific heat ratio of ammonia
R	Gas constant of ammonia
P	Vaporizer pressure
T	Propellant temperature
t	Time
g	Constant of gravity acceleration (9.8 m/s^2)
A	Final equilibrium pressure of vaporizer in the saturated state
B	Impact factor of vaporizer pressure rising slope change rate
C	Impact factor of initial vaporization pressure
T_0	Initial temperature
T_{f}	Final heating temperature
P_0	Initial vaporization pressure
P_1	Initial thrust pressure
P_2	Thrust pulse valley pressure
P_{f}	Saturated vapor pressure at T_{f}
F_1	Thrust pulse peak thrust
F_2	Thrust pulse valley thrust
B_1, B_2, B_3	Parameters of the third-order polynomial fitting
t_1	Thrust pulse width
t_2	Thrust pulse interval
I_{u}	Thrust impulse element of a single thrust pulse
m	Total propellant mass of the propulsion system
m_0	Feedstock mass of the vaporizer in every operation cycle
Δm	Total propellant consumption mass
n_1	Total number of feedstock processes
n_2	Total number of output thrust impulse elements
W	Total power consumption of exhausting the propellant
w_1	Power consumption of the first vaporization process after the feedstock process
w_2	Power consumption of the vaporization process in each thrust pulse interval

completely in this vaporizer in conditions of active thermal and pressure control. With respect to the system structure, the multiplex parallel sieve type vaporizer is processed into a bent structure that is attached to the ammonia tank to reduce the system volume.

Fig. 3a shows the relationship between the components and the operation of the ASVP system procedures. The microcontroller unit (MCU) is the core processor of the propulsion system, which controls four function units: propellant management unit, feedstock control unit, vaporization control unit, and thrust control unit. The following units constitute the self-managed vaporization module of the ASVP system: The propellant management unit monitors the temperature and the pressure of the ammonia tank to ensure the safety of the propellant storage in orbit. The feedstock control unit controls the feed rate and feed time length of the vaporizer. The inflow mass of propellant (namely the product of feed rate and feed time length) is designed to ensure that the gas-liquid mixture in the vaporizer is proportionally saturated (details in Section 3). The vaporization control unit can control and monitor the vaporization state independently according to vaporization requirements. Based on the thrust control

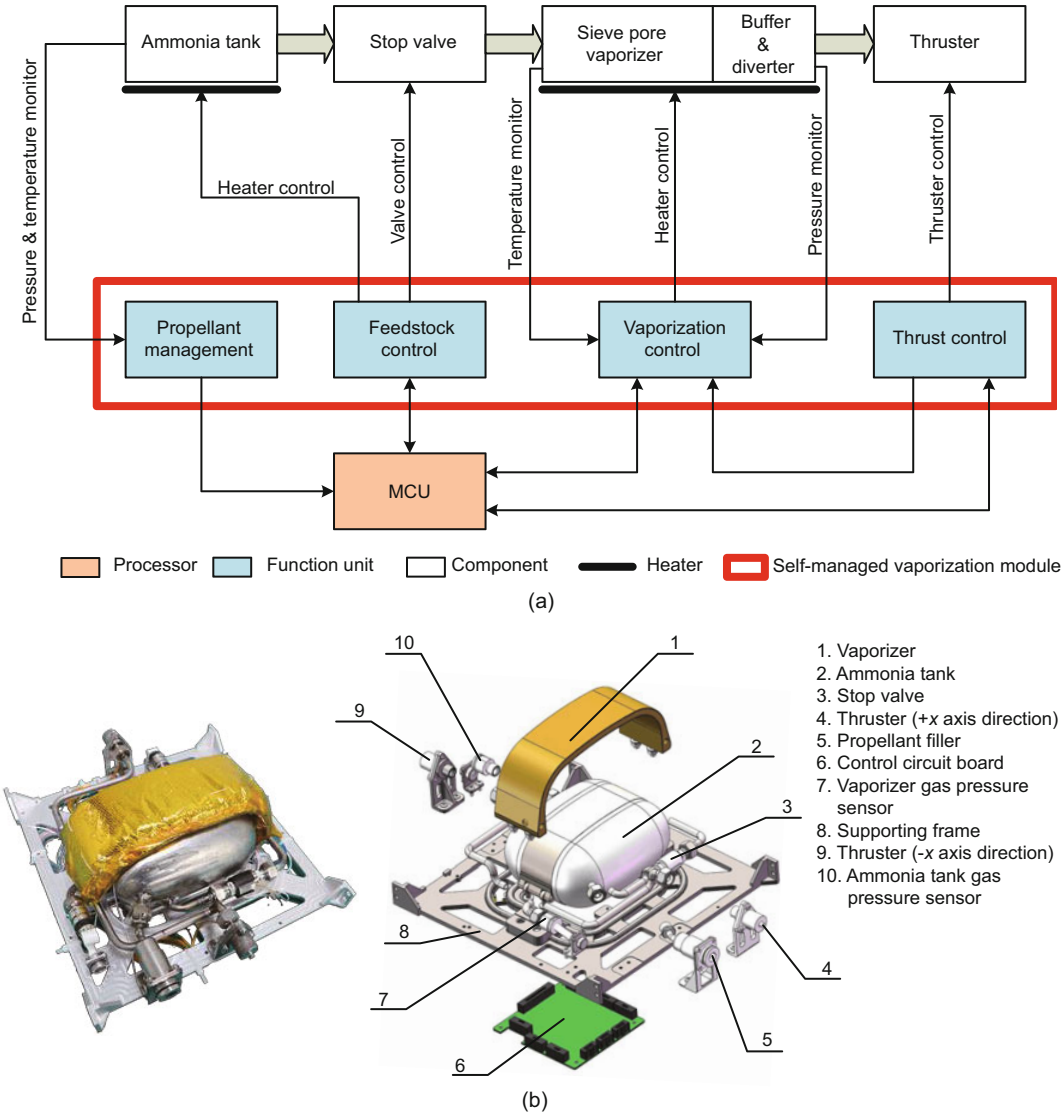

Fig. 3 Ammonia self-managed vaporization propulsion (ASVP) system: (a) control block diagram; (b) physical picture and exploded figure. MCU: microcontroller unit. References to color refer to the online version of this figure

strategy (details in Section 3), the thrust control unit offers the vaporization requirements to the vaporization control unit and controls the thrusters.

A physical picture and an exploded figure of the ASVP system are shown in Fig. 3b. The general indicators of the ASVP system are presented in Table 2.

Table 2 General indicators of the ammonia self-managed vaporization propulsion (ASVP) system

Indicator	Value
Total mass (dry weight) (g)	≤1400
Total mass (wet weight) (g)	≤1800
Outline size (cm^3)	20×20×9
Propellant capacity (L)	0.6
Propellant mass (g)	≥340 (liquefied ammonia)
Supply voltage (V)	3.7–6.0 (typically 4.2)
Standby power (W)	0.2
Peak power (W)	9

3 Thrust control strategy of ASVP

3.1 Basic principles of thrust control

According to the theory of gas dynamics, the output thrust of the Laval nozzle in vacuum (Wu et al., 2016) is

$$F = C_{\mathrm{f}} P_{\mathrm{c}} A_{\mathrm{t}}. \tag{1}$$

In Eq. (1), the thrust coefficient (C_{f}) and the cross-sectional area of nozzle throat (A_{t}) are two parameters related to the design of the thruster, and they are fixed when a certain thruster is selected. Thus, it can be seen that the value of thrust is proportional to the thrust chamber pressure (P_{c}).

On the other hand, specific impulse (Wu et al., 2016) is defined as

$$I_{\mathrm{sp}} = \frac{F}{\dot{m}g}. \tag{2}$$

For the Laval nozzle, the propellant mass flow rate (Wu et al., 2016) is given by

$$\dot{m} = \frac{\Gamma P_{\mathrm{c}} A_{\mathrm{t}}}{\sqrt{RT_{\mathrm{c}}}}, \tag{3}$$

where Γ is a parameter determined by the propellant specific heat ratio k only (Wu et al., 2016).

From the above formulae, we can draw the following conclusions: (1) The thrust value can be controlled by adjusting the thrust chamber pressure; (2) The internal energy of the propellant determines the output specific impulse.

In particular, there is a definite correlation between the thrust chamber pressure and the internal energy of the saturated liquefied gas within a closed container. The pressure (saturated vapor pressure) and the temperature (internal energy) correspond to each other, and also have a positive correlation. Consequently, pressure and temperature control of the propellant is the key of the control of the vaporization process, and will achieve control of output thrust and specific impulse.

3.2 Thrust control procedure

A thrust control procedure is carried out to stably actualize the pressure and temperature control of the vaporizer. The procedure is shown in Fig. 4.

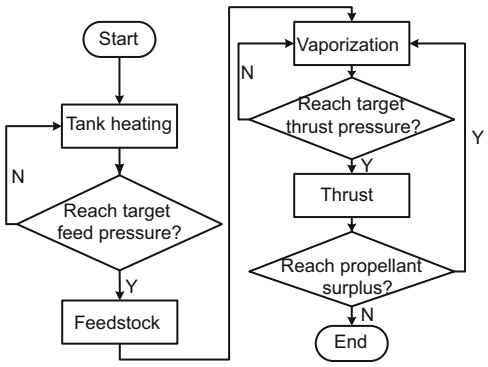

Fig. 4 Thrust control procedure block diagram

The procedure includes three main steps: feedstock, vaporization, and thrust. When the feedstock is completed, the propellant in the vaporizer starts its first vaporization process. The thruster then begins to work, and the next vaporization process will start when the thruster is closed. The thrust process alternates with the vaporization process until the inflow propellant is exhausted. It is a holonomic thrust control procedure from feedstock to the final thrust. To optimize the thrust control strategy, the three stages of the thrust control procedure are rigorously analyzed.

3.2.1 Feedstock control

Feedstock control is implemented mainly by the stop valve and tank heaters. When the stop valve is opened, the pressure difference of the valve throat

will lead the liquefied ammonia flow from the ammonia tank to the vaporizer. The flow rate (also called the feed rate) is determined by the pressure difference between two ends. As the system works in the vacuum (so the vaporizer pressure is zero before the feedstock process), this pressure difference is equal to the ammonia tank pressure. Therefore, the feed rate is determined by the inner pressure of the ammonia tank, which can be controlled by the tank heater.

Based on feedstock ground tests, the gas-liquid mixture will be in the optimized saturation state when the inflow liquefied ammonia volume reaches one-third of the vaporizer capacity (supposing no vaporization occurred). Here, the "optimized saturation state" or "proportionally saturated" has two meanings: (1) The ammonia in the vaporizer is saturated instead of completely vaporized. Under this condition, the inner pressure of the vaporizer will come up to the maximum at the corresponding control temperature. (2) The proportion of liquid in the gas-liquid mixture is not too high to be ejected from the thruster in the gas state only.

The following analyses and tests were conducted based on this optimized saturation state feedstock control.

3.2.2 Vaporization control

We use the mathematical method to analyze and study the vaporization process quantitatively, which is the crux of vaporization control. Based on the thrust control procedure, the vaporization process in the vaporizer occurs in two cases: (1) After the feedstock process, the propellant begins to vaporize to reach the inner pressure that satisfies the thrust requirement. (2) After each thrust process, the propellant vaporizes again to restore the required inner pressure for the next thrust process.

Both cases of vaporization are controlled by highly efficient heaters of constant heating power. According to the heater characteristics, a whole vaporization process begins from an unsaturated state at the initial temperature (T_0) to the saturated state at the final heating temperature (T_f). Fig. 5 shows the whole vaporization process based on the ground test. Each vaporization process that conforms to the initial conditions will obey this law even though the final saturated state is not reached yet.

In Fig. 5, the upper curve shows the variation of the vaporizer pressure and the lower curve shows the

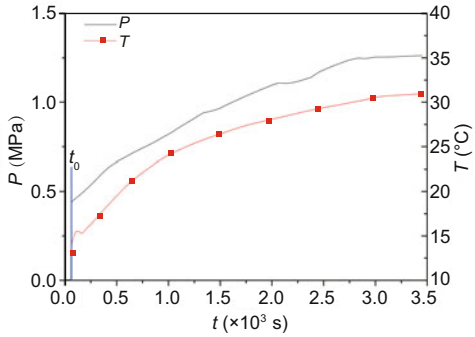

Fig. 5 Evolution curves of measured pressure and temperature during a vaporization process

variation of the propellant temperature during the vaporization process. The vaporizer begins to feed at t_0 and then the vaporization process starts. We can see that the vaporization process starts from the unsaturated state at 5 °C to the nearly saturated state at 31 °C. It is obvious from the curves that the variation of the vaporizer pressure (represented by vaporization regularity) has typical mathematical characteristics. The vaporization regularity can be approximated to a natural exponential function as follows:

$$y(t) = A\mathrm{e}^{-\frac{B}{t+C}} \ (t \geq 0). \tag{4}$$

The corresponding graph of the above function is Fig. 6.

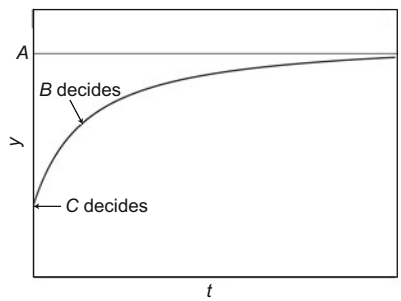

Fig. 6 Graph of the vaporization regularity approximation function

Apparently, this parameter-involved approximation function is quite similar to the measured pressure in Fig. 5. Parameters A, B, and C not only decide the trend of the curve, but have physical meanings related to the vaporization process features (Fu et al., 2005).

A is the final equilibrium pressure of the vaporizer in the saturated state. When the liquefied

ammonia is saturated at the final heating temperature (T_f), the inner pressure of the vaporizer is the final equilibrium pressure (also called the "saturated vapor pressure"). No matter how long it takes, the pressure will not increase further, just like the approximation value A in Fig. 6. Accordingly, the value of A is equal to the saturated vapor pressure at T_f, denoted by P_f (the saturated vapor pressure which can be calculated by the physical chemistry theory).

B is the impact factor of the vaporizer pressure rising slope change rate. During the vaporization process, the rising slope change rate of the pressure is influenced mainly by two factors: the initial internal energy of the propellant and the heating ability (heating power and final heating temperature). On the one hand, the higher the initial internal energy of propellant is, the higher the vaporization rate is, and the faster the curve rises. On the other hand, the stronger the heating ability is, the higher the vaporization rate is, and the faster the curve rises. As can be seen from the curve decided by parameter B in Fig. 6, the value of B is negatively correlated with the rate at which the curve rises. This means B can represent the vaporization rate, which is influenced by the initial internal energy of the propellant and the heating ability.

B is related to T_0 (initial temperature), T_f (final heating temperature), and w (heating power), denoted by $B = f(w, T_0, T_\mathrm{f})$. In addition, all the heaters in the ASVP system have fixed heating power so that w is a constant. As a result, B can be simplified as $B = f(T_0, T_\mathrm{f})$. Among them, T_0 and T_f are monitored by vaporization tests. Therefore, we estimate the value of B to match the measured pressure curves (Table 3).

Derived by the third-order polynomial fitting (the precision has already met the needs of engineering) of estimated B, the expression of $B = f(T_0, T_\mathrm{f})$ is

$$B = \sum_{i=1}^{3} B_i (T_\mathrm{f} - T_0)^i + \text{intercept}. \tag{5}$$

Consequently, the estimated B and the fitted B are listed in Table 4. According to the following ground tests, the regular residuals are acceptable in actual thrust control.

C is the impact factor of initial vaporization pressure. Under the premise that A and B are known, the whole vaporization process is a certain process. However, each vaporization process may begin at an independent initial vaporization pressure P_0 (which is the pressure at the moment $t = 0$). The intercept of the vaporization regularity curve is the initial vaporization pressure, which means that every vaporization curve can be obtained by translation along the time axis of the whole vaporization curve. We can infer the following semi-empirical vaporization regularity formula from Eq. (4):

$$P(t) = P_\mathrm{f} \mathrm{e}^{-\frac{B}{t+C}}. \tag{6}$$

Then we can obtain C by solving the formula above:

$$C = -\frac{B}{\ln(P_0/P_\mathrm{f})}. \tag{7}$$

In conclusion, based on the physical chemistry theory and the ground tests, we propose the semi-empirical vaporization regularity formula in this subsection, which indicates the relationship between vaporization time variation and vaporizer pressure. In Eq. (6), we can obtain the time-varying vapor pressure quantitatively if the initial vaporization pressure P_0, the initial temperature T_0, and the final heating temperature T_f are known. It is applicable simultaneously for the two vaporization cases mentioned at the beginning of this subsection.

Because the vaporization regularity function exhibits a monotone increase, the corresponding abscissa value of the thrust chamber pressure is the vaporization time length that needs to reach a target

Table 3 Values of estimated B under different initial conditions

P_0 (MPa)	T_0 (°C)	P_f (MPa)	T_f (°C)	$T_\mathrm{f} - T_0$ (°C)	Estimated B
1	26	1.3473	35	9	75
0.9	24	1.3473	35	11	100
0.7	15	1.3473	35	20	230
0.6	10	1.3473	35	25	325

B: impact factor of vaporizer pressure rising slope change rate; P_0: initial vaporization pressure; T_0: initial temperature; T_f: final heating temperature; P_f: saturated vapor pressure at T_f

thrust pressure. The thrusters may open at any target thrust pressure even though the final saturated state is not reached yet. The vaporization control unit can calculate the vaporization time from the thrust requirements, control the vaporizer heaters, and monitor the vaporization state, which are the self-managed means of the vaporization process.

Table 4 Values of estimated and fitted B

P_0 (MPa)	Estimated B	Fitted B	Regular residual
1.0	75	77.089 62	−2.089 62
0.9	100	96.837 93	3.162 07
0.7	230	232.575 65	−2.575 65
0.6	325	323.292 48	1.707 52

B: impact factor of vaporizer pressure rising slope change rate; P_0: initial vaporization pressure

3.2.3 Thrust control

The thrust process is essential for the propellant to be ejected from the thruster. The target of the thrust process is to make the output thrust uniform and adjustable. To study it, we carried out an extended thrust test and obtained the following results.

The vapor pressure was also monitored (Fig. 7). As discussed in Section 3.2.1, the thrust value is proportional to the thrust chamber pressure. The conclusion has been verified.

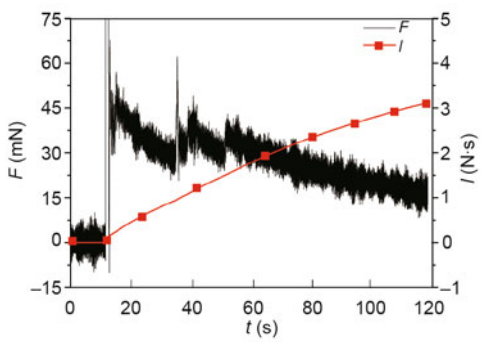

Fig. 7 Thrust and impulse results of the long-period thrust test

Figs. 7 and 8 are the testing results under the initial conditions of propellant temperature at 30 °C and vaporizer pressure at 1.15 MPa. The thrust lasts 100 s. The following conclusions can be drawn from the testing results: (1) The output thrust shows a downward trend; (2) Obvious thrust fluctuations are shown in the thrust curves.

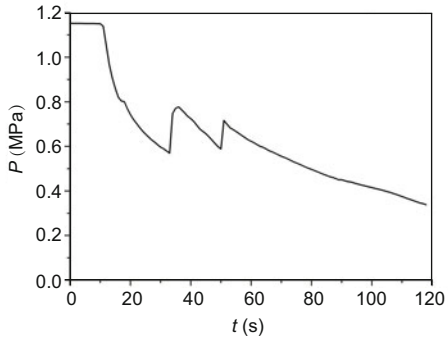

Fig. 8 Vapor pressure monitoring results of the long-period thrust test

The reasons for the phenomena above are as follows: the exhaust velocity is much higher than the vaporization rate, which leads to the minor difference between the pressure of the exhausted space and the vacuum. As a result, there is a marked drop in the global vapor pressure, which is reflected in the thrust value. If the slippage of the thrust value exceeds the threshold, the explosive growth of the liquid molecules and their tendency to escape will cause the gas-liquid two-phase system to vaporize violently. That is the reason why there are strong increases and fluctuations of the thrust.

The thrust instability must be overcome in the thrust control procedure. As we can see from the time-varying curves in Figs. 7 and 8, reducing the thrust time is effective for avoiding thrust fluctuations. Moreover, in a short thrust period, the thrust curve is an approximately straight line, which shows a linear relationship between time variation and thrust. If the propulsion system works in orbit, the short-period thrust closely resembles the instantaneous impulse, which will achieve more efficient orbit control. In consideration of the thrust test-bench response delay, we chose 3 s as the short-period thrust time length to build a high-precision model to fit the exhaust regularity curve.

During the short-period thrust tests, different initial thrust pressures from 0.6 to 1.0 MPa were considered, and we monitored the time-varying pressure variations. The results are shown in Fig. 9.

From the testing results, the pressure is approximately linear with the exhaust time variation, the slope is negative, and the intercept is the initial thrust pressure. Hence, we present the linear fitting results in Table 5.

In conclusion, based on the ground tests, we propose the fitting exhaust regularity formula in Section 3.2.3, which indicates the relationship between the thrust time variation and the vaporizer pressure.

The thrust control procedure is entirely analyzed in Section 3.2. To make the output thrust stable, uniform, and controllable, we used the pulse width modulation (PWM) thrust control strategy. Fig. 10 shows the ideal thrust control strategy curve.

In the strategy, there are three key parameters which determine the thrust control procedure.

1. Initial thrust pressure (P_1)

The value of the thrust is proportional to the thrust chamber pressure which was derived in Section 3.2.1. As a result, the higher the initial thrust pressure is, the higher the initial thrust and the impulse element (for the same pulse width) are. However, the initial thrust pressure cannot be infinitely improved because it is limited by the initial vaporization conditions. P_1 is designed as a comprehensive consideration of the desired thrust, impulse element, pulse interval, power consumption, etc.

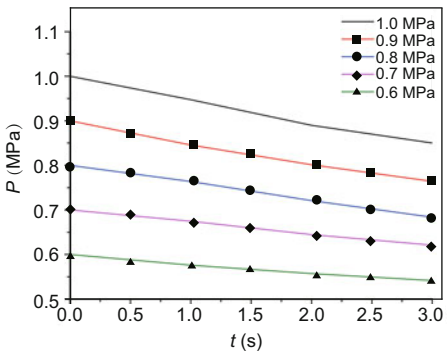

Fig. 9 Actual exhaust pressure curves at different initial thrust pressures

Table 5 Linear fitting results of the actual exhaust pressure curves

P_1 (MPa)	Slope	Intercept	Fitting function $P(t)$
1.0	−0.050 73	0.997 87	$-0.050\,73t+0.997\,87$
0.9	−0.045 24	0.895 64	$-0.045\,24t+0.895\,64$
0.8	−0.039 18	0.800 79	$-0.039\,18t+0.800\,79$
0.7	−0.026 67	0.700 10	$-0.026\,67t+0.700\,10$
0.6	−0.019 43	0.597 90	$-0.019\,43t+0.597\,90$

P_1: initial thrust pressure

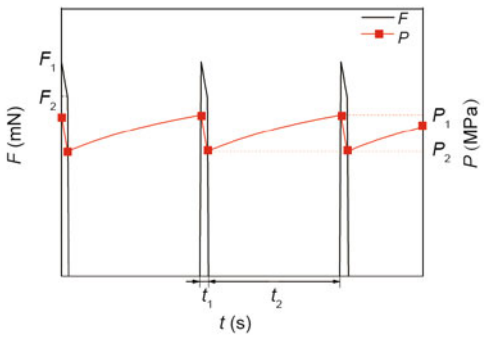

Fig. 10 Pulse width modulation (PWM) thrust control strategy for the ammonia self-managed vaporization propulsion (ASVP) system

2. Thrust pulse width (t_1)

During the thrust pulse width, the vaporizer pressure changes from P_1 to P_2, and the corresponding output thrust changes from F_1 to F_2. If the initial thrust pressure is known, the thrust pulse width determines the value of the thrust impulse element. Considering that the fitting exhaust regularity formula is $P(t)=at+P_1$, the value of the thrust impulse element of the thrust pulse width t_1 is

$$I_{\mathrm{u}}=\int_0^{t_1} C_{\mathrm{f}}A_{\mathrm{t}}P(t)\mathrm{d}t=C_{\mathrm{f}}A_{\mathrm{t}}\left(\frac{1}{2}at_1^2+P_1t_1\right). \quad (8)$$

Eq. (8) depends on the fitting exhaust regularity formula, which means that t_1 should not be larger than the exhaust time in exhaust regularity. As discussed above, $t_1=3$ s.

3. Thrust pulse interval (t_2)

Because the output thrust is supposed to be uniform, all of the thrust pulses should be equal. Accordingly, during the thrust pulse interval between two adjacent thrust pulses, the vaporizer pressure should be back to the initial thrust pressure. In vaporization regularity, the corresponding abscissa value of the target pressure (i.e., the initial thrust pressure) is the vaporization time.

To summarize Section 3.2, we have analyzed the thrust control procedure according to the physical chemistry theory, ground tests, and mathematical fitting methods. Specifically, for the key steps, the vaporization process and the thrust process, we have built two semi-empirical formulae to describe the correspondence between time and the thrust chamber pressure. Based on these analyses, the PWM thrust control strategy for the ASVP system was proposed to achieve stable, uniform, and controllable thrust output. Different parameters of the PWM thrust control strategy will bring different control goals to the ASVP system.

3.3 Optimal thrust control strategy

The power consumption of ASVP is supposed to be efficiently used on account of the resource constraints of micro-nano satellites. In this subsection, we will study the optimal thrust control strategy, to meet the impulse and thrust requirements under the lowest power consumption. In other words, the optimal strategy will achieve the peak conversion efficiency of the power to the thrust impulse.

Consider a certain thrust control strategy, in which the total propellant mass is m, the feedstock mass of the vaporizer in every operation cycle is m_0, the theoretical specific impulse is $I_{\rm spt}$, and the thrust impulse element of a three-second thrust pulse width is $I_{\rm u}$. If the small propellant surplus at the end of a holonomic thrust process is neglected, we can obtain the total numbers of feedstock processes and output thrust impulse elements, which are n_1 and n_2, respectively:

$$n_1 = \frac{m}{m_0}, \tag{9}$$

$$n_2 = \frac{mI_{\rm spt}}{I_{\rm u}} - n_1. \tag{10}$$

If the power consumption of the first vaporization process after the feedstock process is w_1 and the power consumption of the vaporization process in each thrust pulse interval is w_2, the total power consumption (compared with the power consumption of the vaporization process, the power consumption of the thruster is low enough to be ignored) of exhausting the ASVP propellant is

$$W = n_1 w_1 + n_2 w_2. \tag{11}$$

Therefore, the thrust control strategy optimization problem is

$$\begin{cases} \min\limits_{P_1 \in P} W(P_1) = n_1(P_1)w_1(P_1) + n_2(P_1)w_2(P_1), \\ \max\limits_{P_1 \in P} I_{\rm u}(P_1),\ \max\limits_{P_1 \in P} I_{\rm spt}(P_1), \\ P = \{P_1 | 0.6 \le P_1 \le 1\}. \end{cases} \tag{12}$$

In the problem, the theoretical thrust performance indicators can be determined with Eqs. (2) and (8) and are listed in Table 6.

As shown in Table 6, the thrust impulse elements and the specific impulses at different initial thrust pressures do not differ significantly. Thus, the key of the optimization problem is to find the minimum total power consumption. According to the conclusions in Section 3.2.2, we can calculate the time of the first vaporization process and each interval vaporization process. In the design of the ASVP system, the heating power is 7 W; the vaporization process power consumptions at different initial thrust pressures are listed in Table 7.

In light of the tests, $m_0 = 6.725$ g. The total power consumption line chart of exhausting a unit mass (1 kg) of propellant in different thrust control strategies is as follows.

Obviously, in Fig. 11, the initial thrust pressure of the optimal thrust control strategy is 0.7 MPa, at which the lowest total power consumption is achieved.

Table 6 Thrust performance indicators in different thrust control strategies

P_1 (MPa)	$I_{\rm u}$ (N·s)	$I_{\rm spt}$ (s)
1.0	0.1705	114.8
0.9	0.1531	114.5
0.8	0.1372	113.7
0.7	0.1221	112.6
0.6	0.1052	111.7

Table 7 Vaporization process power consumptions in different thrust control strategies

P_1 (MPa)	First vaporization duration (s)	w_1 (J)	t_2 (s)	w_2 (J)
1.0	1614	11 298	85	595
0.9	1223	8561	71	497
0.8	939	6573	61	427
0.7	613	4291	56	371
0.6	359	2513	50	350

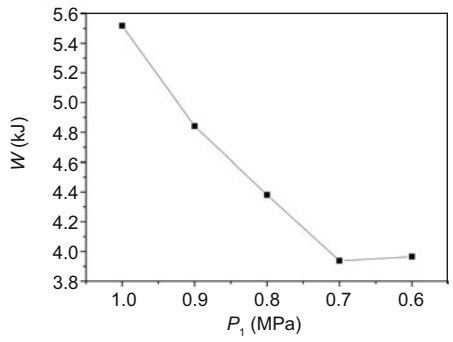

Fig. 11 Total power consumptions in different thrust control strategies

4 Ground test of ASVP

4.1 Introduction of the ground test and related errors

The ground test of the ASVP system was conducted on full elastic micro thrust measurement equipment in vacuum (Tang et al., 2007). The measurement range of the thrust is 0–200 mN with ±1% measurement precision. Based on the equipment performance, test conditions, thrust control method, and data processing method, the ground test errors are derived mainly from the following aspects:

1. The high-frequency jitter of the test results and the response delay of the thrust test-bench could not be avoided or overcome. In this study, low-pass fast Fourier transformation (FFT) filtering and response delay matching correction have been used to reduce the measurement errors as much as possible. However, the thrust test-bench is a full elastic measurement tool, so vibrations appear in the testing results, especially when the thrust drastically changes.

2. The vaporization regularity formula and the exhaust regularity formula were derived by mathematical induction of measurement results. The present precision of the mathematical models is accurate enough to analyze the thrust control procedure quantitatively, but the models are not fit for all liquid-gas transition processes. To make the models generally applicable, higher precision calibration should be implemented for the models in follow-up tests.

3. The pressure and temperature sampling results are the most important parameters in the ASVP system ground test. There are two main sampling error sources: first, the temperature detected by thermocouples and temperature sensors on the surface of the measured objects cannot reflect the real inner temperature. Second, the vaporizer pressure is slightly higher than the thrust chamber pressure at the same moment because there is a pipeline between the vaporizer and the thruster. As a result, deviations are shown in the measured sampling results.

4.2 Theoretical performance of the optimal strategy

The calculation of the theoretical performance parameters of the ASVP system depends on the methods in Section 3.

In the optimal thrust control strategy, the initial thrust pressure is 0.7 MPa and the thrust pulse width is 3 s. Following the exhaust regularity in Table 5, $P_2 = 0.620\,09$ MPa. So, we have

$$F_1 = C_\mathrm{f} P_1 A_\mathrm{t} = 38.65 \text{ mN}, \tag{13}$$

$$F_2 = C_\mathrm{f} P_2 A_\mathrm{t} = 33.66 \text{ mN}. \tag{14}$$

According to Eq. (8), the value of the thrust impulse element for the 3-s thrust pulse width is $I_\mathrm{u} = 0.1221$ N·s.

For the vaporization process, the pressure curve varies and obeys vaporization regularity. The thrust pulse width is so short that the vaporizer inner temperature changes little during the thrust period. Consequently, the initial temperatures of the first vaporization process and each interval vaporization process can be considered identical. According to Tables 3 and 4, the semi-empirical vaporization regularity formula parameters are $B = 232.575\,65$ and $P_\mathrm{f} = 1.3473$ MPa. Another parameter C of each interval vaporization process is

$$C = -\frac{B}{\ln(P_2/P_1)} = 299.6574. \tag{15}$$

In summary, the semi-empirical vaporization regularity formula of each interval vaporization process is

$$P(t) = 1.35\mathrm{e}^{-\frac{232.58}{t+299.66}}. \tag{16}$$

The interval vaporization process regularity curve is shown in Fig. 12.

It can be concluded from the interval vaporization process regularity that the thrust pulse interval is 56 s to restore the initial thrust pressure to 0.7 MPa.

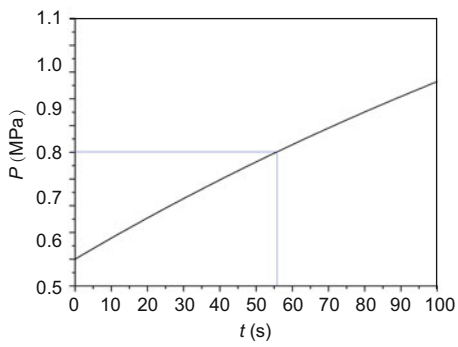

Fig. 12 Interval vaporization process regularity curve of the optimal thrust control strategy

In conclusion, the theoretical performances of the ASVP system using the thrust control strategy are shown in Table 8.

Table 8 Theoretical performances of the ammonia self-managed vaporization propulsion (ASVP) system in the optimal thrust control strategy

Indicator	Value
Initial press (MPa)	0.7
Thrust pulse width (s)	3
Thrust pulse interval (s)	56
Theoretical thrust (mN)	33.66–38.65
Theoretical impulse element (N·s)	0.1221
Theoretical specific impulse (s)	112.6

4.3 Experimental performance of the optimal strategy

We conducted a test of the ASVP system optimal thrust control strategy. Compared with the theoretical optimal thrust control strategy, the thrust pulse interval in the test rises to 60 s to make the liquefied ammonia vaporize more completely. The testing results are shown in Fig. 13.

In the figure, the black line is the thrust curve and the red line is the output total impulse curve. The blue line in Fig. 13 is the peak thrust polyline of 10 thrust pulses. The thrust pulses are obviously uniform, as indicated by both the approximately horizontal peak thrust line and the uniformly increasing total output impulse.

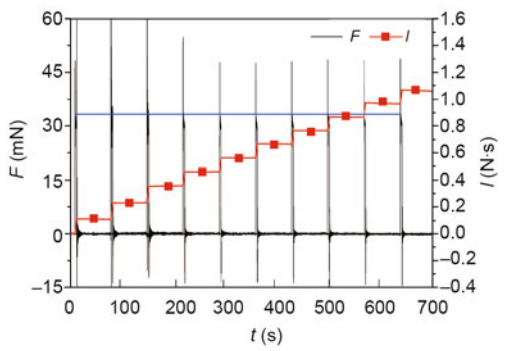

Fig. 13 Thrust testing results in the optimal strategy (10 thrust pulses). References to color refer to the online version of this figure

To clearly describe the details of the thrust pulse, the enlarged thrust output curve of a single pulse is shown in Fig. 14. During the single thrust pulse, it can be seen that the change in the thrust value follows exhaust regularity.

The vaporizer pressure was also monitored (Fig. 15). Combined with the thrust testing results, Fig. 15 illustrates that the output thrust of the ASVP system is stable, uniform, and controllable, which is consistent with the thrust control strategy design.

Instead of the complex propellant mass flow rate measurement, the total propellant mass consumption is used to calculate the specific impulse. The formula is

$$I_{\mathrm{sp}} = \frac{I}{\Delta m}, \tag{17}$$

where I is the total output impulse which can be measured by the thrust test-bench, and Δm is the total propellant mass consumption (namely the mass difference between figures before and after the test).

According to the testing results and the calculations above, the experimental performance of the ASVP system using the thrust control strategy is shown in Table 9.

In conclusion, the results of the ground test and the theoretical calculation reach agreement. By means of credible thrust tests, it was proved that the

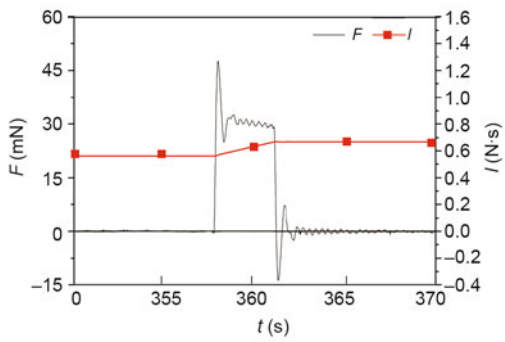

Fig. 14 Output thrust of a single thrust pulse

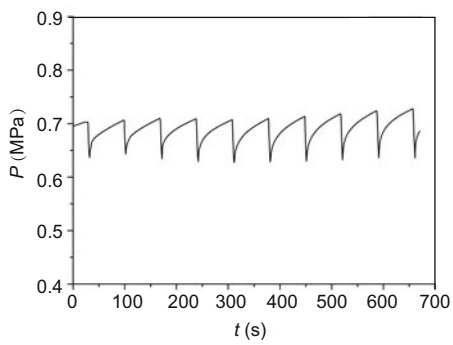

Fig. 15 Measured time-varying pressure in the optimal strategy (10 thrust pulses)

design and the thrust control strategy of the ASVP system are implementable.

Table 9 Experimental performances of the ammonia self-managed vaporization propulsion (ASVP) system in the optimal thrust control strategy

Indicator	Value
Initial press (MPa)	0.7
Thrust pulse width (s)	3
Thrust pulse interval (s)	60
Experimental thrust (mN)	29.80–33.54
Experimental impulse element (N·s)	0.1155
Experimental specific impulse (s)	109.0

5 Conclusions

We have presented the ammonia self-managed vaporization propulsion (ASVP) system to provide a high-impulse density actuator for micro-nano satellites. Compared with other liquefied gas propulsion techniques, the system volume and mass were obviously reduced and the advantage of a high theoretical specific ammonia impulse was put forth sufficiently. Based on the structure of a multiplex parallel sieve type vaporizer and related vaporization process control methods, the ASVP system makes the liquefied ammonia propellant vaporize completely in the self-managed mode. The specific output impulse, which is close to the theoretical specific impulse of ammonia, has been achieved with low power consumption of less than 10 W. The ASVP system advantages of high specific impulse, easy fabrication, and low power consumption offer a suitable choice for small and resource-constrained micro-nano satellites. The indicators contrasting the ASVP system and other representative liquefied ammonia propulsion systems are shown in Table 10.

Based on the ASVP system design, the output thrust and specific impulse are adjustable to meet different mission requirements through control of the vaporization process. The PWM thrust control strategy has been adopted to control the vaporization process effectively, which makes the output thrust stable, uniform, and controllable. In addition, the problem associated with the high heat of vaporization has been solved by the PWM control strategy, which makes the ASVP system applicable to other propellants. Based on the existing design, an optimal strategy was presented to promote the complete vaporization of liquefied ammonia and the peak conversion efficiency of the power to thrust impulse.

The ASVP system presented and investigated in this work provides an efficient and reliable propulsion system for micro-nano satellites and will be verified by the on-orbit operation of ZDPS-3 (the third-generation pico-nano satellite of Zhejiang University) satellites.

Compliance with ethics guidelines

Shu-jian SUN, Tao MENG, and Zhong-he JIN declare that they have no conflict of interest.

References

Carpenter CB, Schmuland D, Overly J, et al., 2013. CubeSat high-impulse adaptable modular propulsion system (CHAMPS) product line development status and mission applications. Proc 45th AIAA/ASME/SAE/ASEE Joint Propulsion Conf, p.1-16. https://doi.org/10.2514/6.2013-3760

Chigier N, Gemci T, 2003. A review of micro propulsion technology. Proc 41st Aerospace Sciences Meeting and Exhibit, p.1-11. https://doi.org/10.2514/6.2003-670

Fu XC, Shen WH, Yao TY, et al., 2005. Phase equilibrium. In: Fu XC, Shen WX, Tao TY, et al. (Eds.), Physical Chemistry (5th Ed.). Higher Education Press, Beijing, China, p.270-280 (in Chinese).

Gibbon D, Charman P, Kay N, 2000. The design, development and in-orbit performance of a propulsion system for the SNAP-1 nanosatellite. Proc 3rd Int Conf on Spacecraft Propulsion, p.91-98.

Gibbon D, Paul M, Smith P, et al., 2001. The use of liquefied gases in small satellite propulsion systems. Proc 37th Joint Propulsion Conf and Exhibit, p.1-7. https://doi.org/10.2514/6.2001-3246

Table 10 Comparison of the ammonia self-managed vaporization propulsion (ASVP) system and other liquefied ammonia mN-level propulsion systems

Propulsion system	Total mass (kg)	Propellant mass (kg)	Total power (W)	Operating mode	Thrust value (mN)	Specific impulse (s)
AMAST P3D	7 (without tanks)	50	800	Arcjet	100	450
YH-1	–	–	50–100	Blow down	120	103
BX-1	2.5	0.74	–	Flashing jet	860	34
ASVP	1.8	0.34	9	PWM	23–74	100–110

Guo SQ, Hou H, Zhang Y, 2013. Propulsion subsystem technology for YH-1 Mars probe. *Aerosp Shanghai*, 30(4):96-99, 245 (in Chinese).
https://doi.org/10.3969/j.issn.1006-1630.2013.04.019

Hejmanowski NJCA, Woodruff RB, 2015. CubeSat high impulse propulsion system (CHIPS). Proc 62nd JANNAF Propulsion Meeting (7th Spacecraft Propulsion), p.1-12.

Lappas V, Pottinger S, Knoll A, et al., 2011. Micro-electric propulsion (EP) solutions for small satellite missions. Proc 2nd Int Conf on Space Technology, p.1-4.
https://doi.org/10.1109/icspt.2011.6064668

Lemmer K, 2017. Propulsion for CubeSats. *Acta Astronaut*, 134:231-243.
https://doi.org/10.1016/j.actaastro.2017.01.048

Levchenko L, Bazaka K, Ding YJ, et al., 2018. Space micropropulsion systems for CubeSats and small satellites: from proximate targets to furthermost frontiers. *Appl Phys Rev*, 5:011104.
https://doi.org/10.1063/1.5007734

Matticari G, Noci GE, Siciliano P, et al., 2006. Cold gas micro propulsion prototype for very fine spacecraft attitude/position control. Proc 42nd AIAA/ASME/SAE/ASEE Joint Propulsion Conf, p.1-13.
https://doi.org/10.2514/6.2006-4872

Poghosyan A, Golkar A, 2017. CubeSat evolution: analyzing CubeSat capabilities for conducting science missions. *Prog Aerosp Sci*, 88:59-83.
https://doi.org/10.1016/j.paerosci.2016.11.002

Ranjan R, Chou SK, Riaz F, et al., 2017. Cold gas micro propulsion development for satellite application. *Energy Proc*, 143:754-761.
https://doi.org/10.1016/j.egypro.2017.12.758

Robin MR, Brogan TR, Cardiff EH, 2008. An ammonia microresistojet (MRJ) for micro satellites. Proc 44th AIAA/ASME/SAE/ASEE Joint Propulsion Conf and Exhibit, p.1-11. https://doi.org/10.2514/6.2008-5288

Satellite Industry Association, 2017. 2017 State of the Satellite Industry Report. Satellite Industry Association, p.18-22. http://www.sia.org [Accessed on Feb. 23, 2017].

Scharfe DB, Ketsdever AD, 2009. A review of high thrust, high delta-V options for microsatellite missions. Proc 45th AIAA/ASME/SAE/ASEE Joint Propulsion Conf and Exhibit, p.1-14.
https://doi.org/10.2514/6.2009-4824

Tang HB, Liu C, Xiang M, et al., 2007. Full elastic microthrust measurement equipment. *J Propul Technol*, 28(6):703-706 (in Chinese).
https://doi.org/10.13675/j.cnki.tjjs.2007.06.023

Wei Q, Li YC, 2012. Technology of ammonia flashing jet propulsion in BX-1 satellite. *Manned Spacefl*, 18(1):86-91 (in Chinese).
https://doi.org/10.3969/j.issn.1674-5825.2012.01.016

Wu XS, Chen J, Wang D, 2016. Foundation of one demensional steady flow. In: Wu XS, Chen J, Wang D (Eds.), Gas Dynamics of Solid Propellant Rocket Motor. Beihang University Press, Beijing, p.32-58 (in Chinese).

Zube DM, Messerschmid EW, 1993. ATOS-flight experiment for a 700W ammonia arcjet. Proc 29th AIAA/ASME/SAE/ASEE Joint Propulsion Conf and Exhibit, p.1-13.
https://doi.org/10.2514/6.1993-2224